PHYSICAL REVIEW B

CONDENSED MATTER

THIRD SERIES, VOLUME 50, NUMBER 15 15 OCTOBER 1994-I

Degenerate Anderson impurity model in the presence of spin-orbit and crystal-field splitting

J. Bonča and J. E. Gubernatis

Theoretical Division and Center for Nonlinear Studies, Los Alamos National Laboratory, Los Alamos, New Mexico 87545

(Received 2 February 1994)

Using a quantum Monte Carlo technique combined with the method of maximum entropy, we calculated the magnetic susceptibility and spectral properties of the degenerate single-impurity Anderson model in the presence of spin-orbit and crystal-field splitting. At small hybridization and moderate temperatures, the magnetic susceptibility displays a nonuniversal behavior. Under the influence of spin-orbit splitting, the magnetic susceptibility decreases due to the quenching of a sixfold-degenerate state to an effectively doubly degenerate state. The effect of crystal-field splitting on the magnetic susceptibility is less pronounced. The temperature dependence of the spectral function changes dramatically under the influence of spin-orbit splitting. In the accessible temperature regime, the central peak at $\omega \sim 0$ decreases with decreasing temperature.

I. INTRODUCTION

The single-impurity Anderson model[1] is a central paradigm for dilute magnetic alloys and related strongly correlated electronic systems. Over the years significant progress has been made in understanding its physical properties because of a gradual development of sophisticated analytical and numerical techniques. The first major development beyond perturbation theory was made by Krishna-murty, Wilkins, and Wilson[2] who used the numerical renormalization group (NRG) to calculate various static properties of the spin-degenerate model. Subsequently, analytical solutions for the ground-state properties were obtained by the Bethe-ansatz technique.[3] Further, the numerical renormalization-group approach was recently extended to calculate dynamic properties for the orbital-degenerate model at zero temperature.[4] Finite-temperature analytical results for dynamic properties are generally provided by the noncrossing approximation (NCA).[5] Recently, Costi and Hewson generalized Wilson's numerical renormalization-group approach to allow calculation of the dynamic properties of the spin-degenerate Anderson model at finite temperatures.[6]

To compare theory to experiment, the introduction of spin-orbit and crystal-field splittings into the model is necessary. There have been several notable analytical and numerical efforts in this regard. From an expression for the Kondo temperature in the presence of crystal fields derived from scaling theory, Yamada[7] explained why Kondo effect dominates intersite Ruderman-Kittel-Kasoya-Yosida (RKKY) interactions in some Ce- and Yb-based dense Kondo systems. Schlottmann[8] solved the Bethe-ansatz equations in the limit $U \rightarrow \infty$ for the ground state of a cerium atom in the presence of crystal-field splitting. He argued that the main effect of the splitting is quenching the $SU(6)$ Kondo state to an effective $SU(2)$ or $SU(4)$ state due to symmetry-breaking crystal fields. In addition, NCA calculations[5] have provided insight into the effects of the spin-orbit splitting on the spectral properties of the model. These calculations predict that the higher-lying multiplets cause the low-energy spectral weight to be much less temperature dependent than expected on the basis of degenerate model.

On the numerical side, Lin and Hirsch[9] used a specifically developed quantum Monte Carlo (QMC) simulation technique (the Hirsch-Fye method[10]) to study the static susceptibility and local-moment formation of a doubly degenerate parametrization of the model. They chose the degeneracy $N=4$ and grouped the four values of the impurity energy levels ϵ_m into two groups of doubly degenerate states, i.e., they took $\epsilon' \equiv \epsilon_1 = \epsilon_2$ and $\epsilon'' \equiv \epsilon_3 = \epsilon_4$. To mimic the crystal-field splitting Δ_{cf}, they chose values of $\epsilon'' = \epsilon' + \Delta_{cf}$. Their main finding was that the static magnetic susceptibility follows a universal curve as a function of T/T_K.[2] Recently, Takegahara[11] used the Hirsch-Fye method to study the sixfold-

degenerate model in the presence of a cubic crystal-field splitting, which corresponds to the ground state of Ce impurity with $j=\frac{5}{2}$. In the presence of these fields, the sixfold-degenerate ground state splits into a Γ_7 doublet and a Γ_8 quartet.[12]

These various analytical and numerical approaches have illustrated that the single-impurity Anderson model successfully describes the formation and screening of the magnetic moment at low temperatures. For dynamical properties the NCA and NRG approaches agree on the main properties of the spectral density function of the degenerate model, such as the position of the broad side peaks and the existence of a sharp resonance close to the Fermi energy; however, the NCA is limited to very large U and N, and the NRG to very low temperatures. There is a need for a method which calculates the spectral properties of the Anderson model at an arbitrary set of parameters and with the presence of spin-orbit and crystal-field splittings. In many respects, the quantum Monte Carlo method fulfills this need.

In this paper, we will present QMC calculations, based on the Hirsch-Fye method, of the properties of the degenerate single-impurity Anderson model in the presence of spin-orbit and crystal-field splittings. When combined with the maximum entropy method, the QMC method has been very successful in calculating spectral properties of the spin-degenerate[13] and orbitally degenerate Anderson models.[14] Its main advantages are that there are no restrictions to infinite or large Coulomb repulsion U, or to large degeneracy N. In addition, there are no finite-size effects since the method offers an exact treatment of an impurity coupled with an infinite sea of conducting electrons. The only systematic numerical error comes from discretizing imaginary time when evaluating the imaginary-time path integral representing the partition function. Its limitations are mainly practical ones: The discretizing prohibits treating large U, and an effective N^3 scaling of the computer time limits the size of N conveniently studied. As a direct result of the method is the production of the impurity part of the many-body, imaginary-time Green's function. To obtain the impurity part of the spectral real-frequency function, we then perform the analytic continuation with the use of the maximum entropy method which combines the method of Bayesian statistical inference with the principle of maximum entropy.[13] Consequently, by modeling spin-orbit and crystal-field splittings, we extend toward experiment our previous calculation of the dynamical properties of the degenerate model. By treating dynamical properties, we step beyond the recent calculations of Takegahara. Our most interesting finding is the nonuniversal behavior of the spectral function as the temperature is lowered and the properties of the model cross over from behavior determined by $N=6$ to behavior determined by $N=2$. As we will discuss more fully, finding the expected $N=2$ universal behavior would require a larger scale calculation than presently practical. We also found that the effect of the crystal-field splitting on the magnetic susceptibility is much smaller than the effect of a somewhat artificial implementation of the spin-orbit splitting of the same magnitude.

We organized this paper as follows: In Sec. II, we briefly discuss the model, the QMC method, and the maximum entropy method. We used the QMC algorithm we previously developed for the orbital-degenerate case,[14] and allowed the input parameters to model the presence of spin-orbit or crystal-field splittings. In Sec. III, we present results for susceptibility and spectral functions. We discuss the influence of spin-orbit and crystal-field splittings on the susceptibility curve. We also investigate the behavior of susceptibility under the spin-orbit splitting in the region of small hybridization. In Sec. IV, we summarize our results.

II. FORMULATION

A. The model

We treated the following form of the degenerate Anderson model:[5]

$$H=H_0+H_1 , \tag{1}$$

where

$$H_0=\sum_{km}\epsilon_k n_{km}+\sum_{km}V_{km}(c_{km}^{\dagger}f_m+f_m^{\dagger}c_{km})+\sum_m \epsilon_m n_m ,$$
$$H_1=\tfrac{1}{2}\sum_{m,m'}U_{mm'}n_m n_{m'} . \tag{2}$$

Here $c_{km}^{\dagger}$ creates a state in the conduction band with the energy ϵ_k, and $f_m^{\dagger}$ creates a state m at the impurity site with the unrenormalized energy ϵ_m. The hybridization of the conducting band with the impurity site V_{km} does not mix states with different m; therefore, the impurity state with the unrenormalized energy ϵ_m that is created by $f_m^{\dagger}$ possesses the same rotational symmetry m as the conducting band. The operators n_{km} and n_m are the number operators for the conduction band and orbitals at the impurity site. We will assume that the conduction band is infinitely wide and structureless; therefore, V_{km} is neither energy nor channel dependent. This assumption leads to the simple relation for the impurity level halfwidth $\Gamma=\pi N(0)V$, where $N(0)$ is the energy density of states per channel at the Fermi energy. In (2), the symmetric matrix $U_{mm'}$, with the additional condition $U_{mm}=0$, represents the Coulomb repulsion between two electrons occupying different orbitals at the impurity site. The method in principle allows for assigning different Coulomb repulsions between different states m. For example, we could choose the Coulomb repulsion within the states of the same multiplet to be larger than the one between the multiplets. We did not exploit this flexibility. Since the highest degeneracy we achieved is $N=6$, we chose to simulate spin-orbit splitting as if the orbital angular momentum of the impurity was $l=1$, which after strong $\vec{l}\cdot\vec{s}$ coupling gives a low-lying doubly degenerate state with total angular momentum $j_1=\frac{1}{2}$ and a higher-lying fourfold-degenerate state with $j_2=\frac{3}{2}$. Different channels m represent different components of total angular momentum; in particular for the low-lying doublet $m_D=-\frac{1}{2}$ and $\frac{1}{2}$, and for quadruplet $m_Q=-\frac{3}{2}$, $-\frac{1}{2}$, $\frac{1}{2}$,

and $\frac{3}{2}$. The nature of the splitting (low-lying doublet and quadruplet) closely resembles the cubic crystal-field splitting of the f level of a Ce impurity atom, where the low-lying sixfold-degenerate state $j=\frac{5}{2}$ splits into the double degenerate Γ_7,

$$\psi_1=\alpha|\tfrac{5}{2}\rangle-\beta|-\tfrac{3}{2}\rangle\ ,$$
$$\psi_2=\alpha|-\tfrac{5}{2}\rangle-\beta|\tfrac{3}{2}\rangle\ , \tag{3}$$

and the fourfold degenerate Γ_8,

$$\psi_3=\beta|\tfrac{5}{2}\rangle+\alpha|-\tfrac{3}{2}\rangle\ ,$$
$$\psi_4=\beta|-\tfrac{5}{2}\rangle+\alpha|\tfrac{3}{2}\rangle\ , \tag{4}$$
$$\psi_{5,6}=|\pm\tfrac{1}{2}\rangle\ ,$$

where $\alpha=\sqrt{\frac{1}{6}}$ and $\beta=\sqrt{\frac{5}{6}}$. Clearly, states Γ_7 and Γ_8 are not eigenstates of j or j_z.[12] The only difference between the spin-orbit and physically more relevant crystal-field splittings is in the rotational symmetry of the states, which changes the properties of the magnetic susceptibility; however, this difference does not affect the impurity part of the spectral function.

B. Methods

The quantum Monte Carlo method we used is identical to the one originally developed to treat the single-impurity, spin-degenerate ($N=2$) Anderson model,[10] and later generalized to treat the doubly spin-degenerate Anderson model.[9] We, as Takegahara, recently extended the method to treat arbitrary degeneracy.[14] Here we summarize its key features.

Key features include dividing the imaginary-time scale into L discrete time intervals $\Delta\tau=\beta/L$, writing a path-integral formulation for the partition function as

$$Z=\mathrm{Tr}e^{-\beta H}=\mathrm{Tr}\prod_{l=1}^{L}e^{-\Delta\tau H}\simeq\mathrm{Tr}\prod_{l=1}^{L}e^{-\Delta\tau H_0}e^{-\Delta\tau H_1} \tag{5}$$

and introducing Hubbard-Stratonovich variables[10] into each factor, and then tracing over fermionic degrees of freedom exactly for a fixed configuration of the auxiliary fields to rewrite the partition function (5) as

$$Z=\mathrm{Tr}_\sigma\prod_{m=1}^{N}\det O_m(\{\sigma\}). \tag{6}$$

The inverse of the matrix O_m is the one-particle Green's function as a function of discrete values of τ. A Monte Carlo method is used to calculate the trace of the Hubbard-Stratonovich variables.

The method thus produces the single-particle Green's function as its natural product. It is the exact Green's function, within the small controllable systematic error caused by the Trotter approximation (5), because the Hubbard-Stratonvich transformation converts the interacting problem into an noninteracting problem which is, of course, solvable.

The imaginary-time Green's function $G(\tau)$ is directly connected to the spectral function $A(\omega)$ by

$$G(\tau)=\int_{-\infty}^{+\infty}d\omega\frac{e^{-\tau\omega}}{1+e^{-\beta\omega}}A(\omega)\ , \tag{7}$$

where β is the inverse temperature. In the case of particle-hole symmetry, the Green's function obeys the relation $G(\tau)=G(\beta-\tau)$. Therefore, $A(\omega)$ is an even function of frequency and also satisfies the sum rule. $\int_{-\infty}^{+\infty}d\omega A(\omega)=1$.

Bayesian statistical inference, with the principle of maximum entropy, yields procedures that enable one to find $A(\omega)$ from $G(\tau)$. The approach is based on probability theory and relies on the specification of probability and conditional probability functions connected by Bayes's theorem. The principle of maximum entropy uses the *a priori* knowledge that the spectral density is non-negative and normalizable (i.e., it satisfies a sum rule), and it enters the process by specifying the prior probability of the spectral density as

$$\Pr[A]\propto e^{-\alpha S}\ , \tag{8}$$

where

$$S=\sum_i[A_i-m_i-A_i\ln(A_i/m_i)]\ . \tag{9}$$

The function m_i is called the model, and it sets the zero of the entropy S. Our results are calculated from[13,15]

$$\langle A\rangle=\int d\alpha\,\Pr[\alpha|G,m]A(\alpha)\ , \tag{10}$$

where the conditional probability function $\Pr[\alpha|G,m]$ is found by using Bayes's theorem. Details are given elsewhere,[13] but the main ingredient, besides (8), is the choice of the likelihood function

$$\Pr[G|A]\propto e^{-\chi^2/2}\ , \tag{11}$$

where χ^2 is the least-squares function

$$\chi^2=\tfrac{1}{2}\sum_{ik}\left[G_i-\sum_j K_{ij}A_j\right]C_{ij}^{-1}\left[G_k-\sum_j K_{kj}A_j\right]\ , \tag{12}$$

with K_{ij} being the kernel from Eq. (7), and C_{ij} the covariance matrix[13] for the different τ components of $G(\tau)$.

III. RESULTS

In this section we present results for the magnetic susceptibility and the spectral functions obtained by QMC simulations for the sixfold-degenerate Anderson model in the presence of spin-orbit and crystal-field splittings. Unless indicated otherwise, we performed calculations with the hybridization $\Gamma=0.125$ and imaginary time step $\Delta\tau=0.125$. We also used two different Coulomb interaction strengths $U=2$ and 4, and split the on-site energies in the following ways: (a) in the case of spin-orbit splitting, the energy of the $j_1=\frac{1}{2}$ states is $\epsilon_D=\epsilon_f-\Delta_{\mathrm{so}}$ and the energy of the $j_2=\frac{3}{2}$ states $\epsilon_Q=\epsilon_f=-1$; and (b) in the case of crystal-field splittings, $\epsilon_{\Gamma_7}=\epsilon_f-\Delta_{\mathrm{cf}}$ and $\epsilon_{\Gamma_8}=\epsilon_f$.

A. Crystal-field magnetic susceptibility

We calculated the magnetic susceptibility χ from

$$T\chi=\int_0^\beta d\tau\langle J_z(\tau)J_z(0)\rangle\ , \tag{13}$$

where J_z is

$$J_z(\tau)=\sum_{m=1}^{N} w(m,m)n_m(\tau) . \quad (14)$$

In the spin-orbit case, w is diagonal: $w(m,m)=-\frac{1}{2}, \frac{1}{2}, -\frac{3}{2}, -\frac{1}{2}, \frac{1}{2}$, and $\frac{3}{2}$ for $m=1-6$. In the case of crystal-field splitting, $w(m,m')=\frac{1}{2}\langle\psi_m|f_s^{\dagger}\sigma^z_{ss'}f_{s'}|\psi_{m'}\rangle$, where ψ_m represent states Γ_7 and Γ_8 in (3) and (5), and $\sigma^z_{ss'}$ is the Pauli matrix.

The magnetic susceptibility (13) was calculated from the Green's function by Wick's theorem

$$J_z(\tau)J_z(0) =J_z(0)^2+\sum_{m,m'=1}^{N} w(m,m')^2[\delta(\tau)-G_m(-\tau)]G_{m'}(\tau) . \quad (15)$$

We reached temperatures as low as $T=\frac{1}{12}$, in which case for $\Delta\tau=0.125$, the maximum number of time slices was $L=\beta/\Delta\tau=100$. In contrast to our previous work,[14] we were unable to reach temperatures smaller than T_K due to smaller, more physical choice of hybridization Γ. We note that the computing time for the Hirsch-Fye algorithm scales as L^3N^2. In addition, the enlarged phase space, which is a consequence of higher degeneracy N, makes it more difficult to equilibrate the simulation and produce statistically independent measurements. These factors increased the computation time by an additional factor of N, so our total computational time scaled as $(LN)^3$.

Defining a sweep as making a Monte Carlo step for each m at all values of l, we used 10 000 sweeps in a bin and skipped nine sweeps between measurements to reduce correlations between measurements. Therefore, the number of measurements within a bin was 1000, and we calculated between 400 and 1000 bins depending on temperature and spin-orbit splitting. At each measurement step, we calculated the one-particle, imaginary-time Green's function and various static correlation functions such as the static magnetic susceptibility, average impurity occupancy, and local moment. For the model in Eq. (9) we used a normalized Lorentzian, centered at $\omega=0$ with the width of the order of 2Γ. The spectral density was for a sufficiently large number of good model-independent data.

All our calculations were performed on a cluster of 16 IBM/RS6000-560 work stations, whose performance was equivalent to roughly $1\frac{1}{2}$ times that of one CPU unit of a Cray Y-MP computer. Our computation times ranged from 4 h to five days.

B. Spin-orbit magnetic susceptibility

In Fig. 1 we present magnetic susceptibilities $T\chi_{so}$ at three different hybridization strengths Γ as a function of temperature. We normalized $T\chi_{so}$ to its high-temperature value

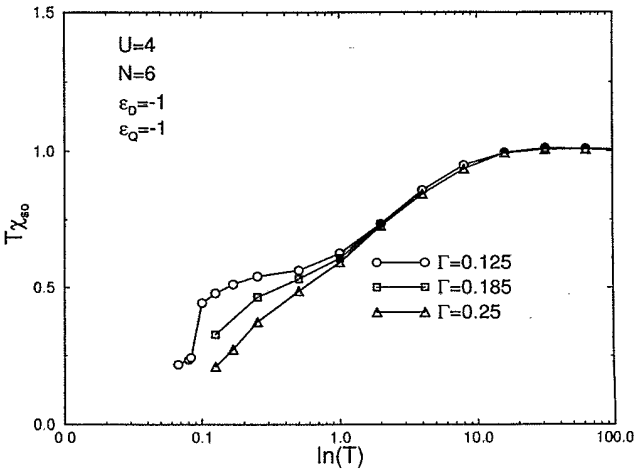

FIG. 1. The susceptibility $T\chi_{so}$ in units of its high-temperature value $\lim_{T\to\infty}T\chi_{so}=\frac{11}{8}$ as a function of $\ln(T)$ calculated for different hybridization strengths Γ. In this and the figures below, the estimated statistical errors are smaller than the height of the markers.

$$\lim_{T\to\infty}T\chi_{so}=\langle J_z^2\rangle_{T\to\infty}=\frac{j_1(j_1+1)}{3}\frac{(2j_1+1)}{4} +\frac{j_2(j_2+1)}{3}\frac{(2j_2+1)}{4} , \quad (16)$$

which equals $\frac{11}{8}$ at $j_1=\frac{1}{2}$ and $j_2=\frac{3}{2}$. As Γ becomes smaller, we observe more structure in the $T\chi_{so}(T)$, indicating that $T\chi_{so}$ curves do not follow universal curves. This behavior is a consequence of the well-known fact that the Kondo temperature T_K decreases exponentially with $1/\Gamma$. Therefore, as Γ decreases, the Kondo regime moves to smaller temperatures. The lowest temperatures reached in our simulations are simply not low enough to investigate the universal behavior. The well-pronounced hump at small $\Gamma=0.125$ is easily explained: at temperatures slightly above T_K, when the local moment is not yet screened by the conducting band electrons, only the lowest multiplet contributes to the ground state. In particular, for the given choice of parameters, the ground state consists of a single occupied state f^1 with some admixture of f^0. We can compute magnetic susceptibility approximately for temperatures far above T_K and small hybridization $\Gamma\ll\epsilon_f$ and U by taking into account contributions of the f^0 and f^1 states with Boltzmann weights. This calculation gives $\chi_{so}\sim\langle J_z^2\rangle\sim0.9$. To compare this result with Fig. 1, the value $T\chi_{so}\sim0.9$ has to be rescaled by its high-temperature limit, $\lim_{T\to\infty}/T\chi_{so}=\frac{11}{8}$. The hump in the susceptibility curve is approximately 15% lower than our estimate. This disagreement is due to finite hybridization. As hybridization increases, the structure in $T\chi_{so}$ (Fig. 1) becomes less pronounced, since a stronger coupling of the impurity with the conducting band leads to stronger screening of the local moment.

In Figs. 2(a) and 2(b), we present $T\chi_{so}(T)$ and $T\chi_{cf}(T)$ for finite spin-orbit and crystal-field splittings, respective-

ly. For the sake of comparison, we chose equal values for spin-orbit and crystal-field splittings, $\Delta_{so}=\Delta_{cf}=0.3$. In both cases, doubly degenerate states lie below the fourfold-degenerate states. The curves are normalized to its high-temperature values where $\lim_{T\to\infty} T\chi_{so}=\frac{11}{8}$ differs from $\lim_{T\to\infty} T\chi_{cf}=[j(j+1)/3][(2j+1)/4]=\frac{35}{8}$.

The effect of the spin-orbit splitting on the magnetic susceptibility is similar to the effect of increased hybridization that was illustrated in Fig. 1. $T\chi_{so}$ for $\Delta_{so}>0$ lies below the curve at $\Delta_{so}=0$. We do not believe, however, that this similarity is a consequence of increasing T_K with the increasing splitting Δ_{so} as suggested recently by Takegahara[11] for the case of small Δ_{cf}. The decrease of $T\chi_{so}$ has a very simple explanation: As the temperature becomes comparable to Δ_{so}, the occupation of the low-lying doublet increases in comparison with the occupation of the excited $j=\frac{3}{2}$ state in a manner roughly following Boltzmann statistics. This depletion of the excited state leads to a decrease in $\langle J_z^2\rangle$ and consequently to a decrease in $T\chi_{so}$.

The effect of crystal-field splitting on magnetic susceptibility $T\chi_{cf}$ observed in Fig. 2(b) is much smaller than in the case of spin-orbit splitting. To clarify this rather unexpected behavior, we calculated the average occupancy of the states with a definite component of the total angular momentum $|j_z|=\frac{1}{2}$, $\frac{3}{2}$, and $\frac{5}{2}$ as a function of temperature in the presence of the crystal-field splitting. The results are presented in Fig. 3. In the same figure, we also present the occupancy per channel $\langle n(\Delta_{cf}=0)\rangle$ in the case of $\Delta_{cf}=0$. As a consequence of the crystal-field splitting the average occupancy $\langle n_{3/2}\rangle$ of the $|j_z|=\frac{3}{2}$ state at low temperatures lies well above $\langle n_{5/2}\rangle$ and $\langle n_{1/2}\rangle$. However, the weight with which the states $|j_z|=\frac{3}{2}$ contribute to the magnetic moment, and consequently to $T\chi_{cf}$, is only $\frac{9}{25}$ of the weight of the $|j_z|=\frac{5}{2}$ states. This effect leads to a small change of $T\chi_{cf}$ in the presence of the crystal-field splitting.

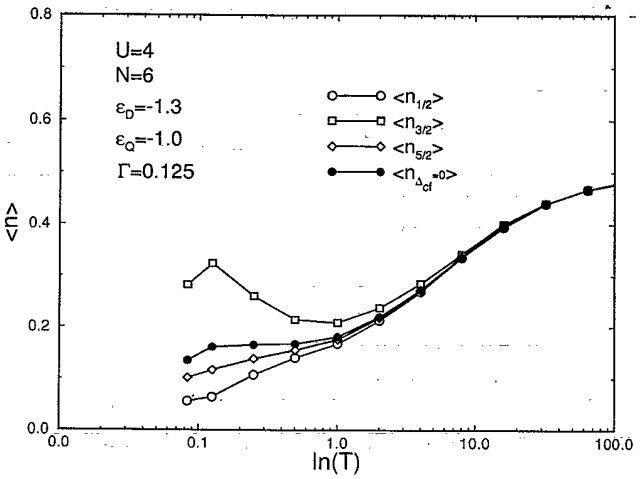

FIG. 3. The average occupancies of levels with definite components of angular momentum j_z in the presence of crystal-field splitting. Also presented is the average occupancy per state m without any splitting $\langle n(\Delta_{cf}=0)\rangle$.

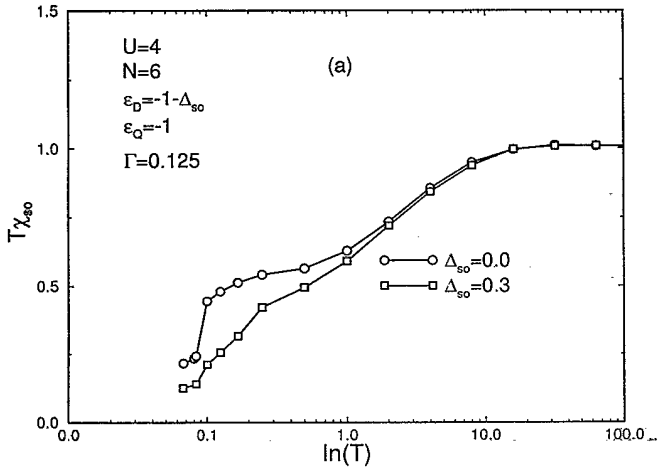

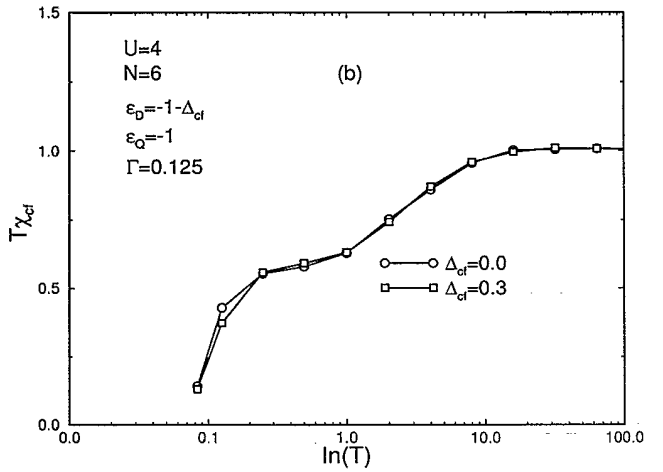

FIG. 2. The magnetic susceptibilities normalized to their high-temperature values as functions of ln(T) presented at zero and finite (a) spin-orbit and (b) crystal-field splitting.

C. Spectral densities

We now turn to an investigation of the spectral properties of the one-impurity Anderson model. First, we note that spectral functions do not depend on the magnetic properties of the states as long as the degeneracy of low- and high-lying states remains unchanged. We investigated two different strengths of splittings, $\Delta_{so}=0.3$ and $\Delta_{cf}=0.1$, which in real materials approximately correspond to spin-orbit and crystal-field splittings, respectively.

In Figs. 4(a) and 4(b), we plot spectral functions of the degenerate Anderson model for $U=2$ and 4 without any splitting. In both cases, the ground state is singly occupied (f^1). The peak with the largest spectral weight, centered approximately at $\omega\sim U+\epsilon_f$, is in both cases well pronounced and corresponds to transition $f^1\to f^2$. We observe a slight temperature dependence of this $\omega>0$ side peak. The peaks in the vicinity $\omega=0$ are a consequence of the formation of the Kondo singlet and represent the

transition $f^0 \rightarrow f^1$. The later peaks are much less pronounced in the case of smaller Coulomb interaction $U=2$ [Fig. 4(a)] than in the case of $U=4$ which is due to the lower Kondo temperature in the case of smaller U. In both cases, the heights of the central peaks increase with a lowering of the temperature, which is the expected behavior. The side peak at negative frequencies, corresponding to transition $f^1 \rightarrow f^0$, is centered around $\omega=\epsilon_f$ and is much less pronounced than its $f^1 \rightarrow f^2$ counterpart. The height and the position of the side peak also vary slightly with temperature. In Fig. 4(b), we clearly see that lowering the temperature moves the side peak toward the central $\omega=0$ peak.

Figures 5(a) and 5(b) present spectral functions at finite spin-orbit splitting $\Delta_{so}=0.3$ with the atomic f-level energies $\epsilon_D=\epsilon_f-\Delta_{so}$ and $\epsilon_Q=\epsilon_f$. All other parameters are the same as in Fig. 4. Comparing Figs. 4(a) and 5(a), we observe in Fig. 5(a) a strong decrease in the height and the spectral weight of the central $\omega=0$ peak, which is a result of a decreased Kondo temperature caused by the finite splitting. The spectral weight and height of the $f^1 \rightarrow f^2$ peak increases, absorbing the loss in spectral weight at small frequencies. Comparing Figs. 4(b) and

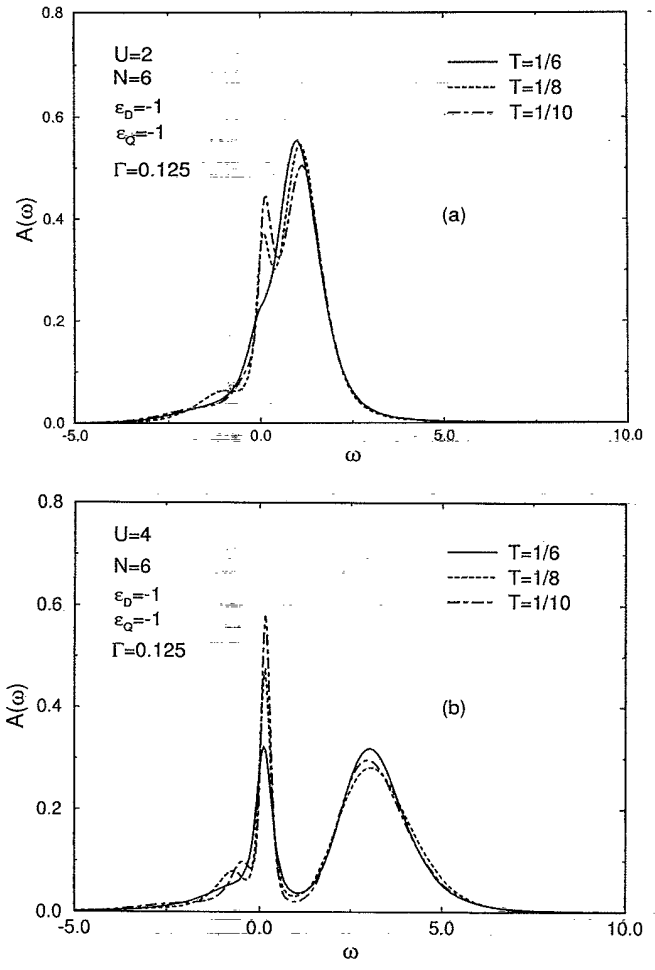

FIG. 4. The spectral densities $A(\omega)$ as functions of the frequency ω without splitting calculated at (a) $U=2$ and (b) $U=4$. Spectral functions are calculated at three different temperatures.

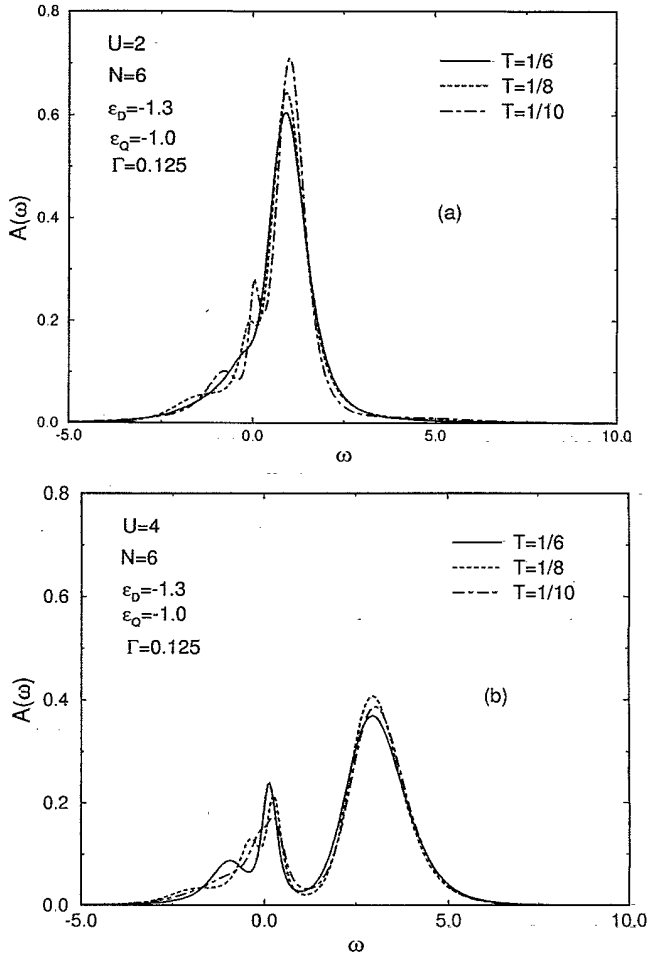

FIG. 5. The spectral densities $A(\omega)$ as functions of the frequencies ω in the presence of spin-orbit splitting calculated at (a) $U=2$ and (b) $U=4$.

5(b), we discover in Fig. 5(b) an even more striking effect of the spin-orbit splitting. Besides a decrease in height and spectral weight of the $\omega=0$ peak, we observe an unusual temperature dependence. In contrast with the zero splitting case in Fig. 4(b), the central peak in Fig. 5(b) decreases with decreasing temperature. We specu-

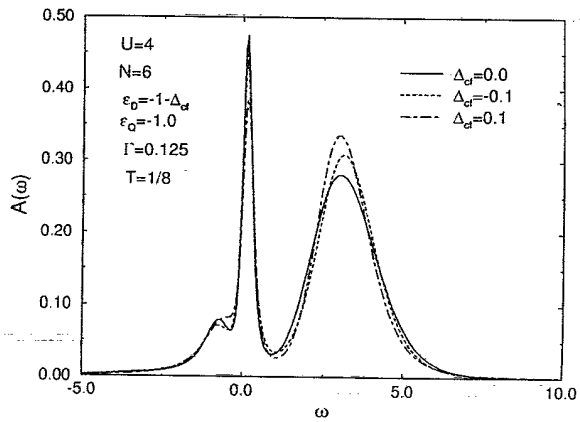

FIG. 6. The spectral densities $A(\omega)$ as functions of the frequency ω in the presence of different crystal-field splittings.

late that this behavior is due to the existence of two different low-energy scales in the system. At higher temperature, a small spin-orbit splitting is "washed out" by temperature fluctuations; therefore, the sixfold degeneracy is restored. As the temperature is lowered, the splitting becomes important, which in our case quenches the degeneracy from 6 to 2. The existence of two different effective degeneracies leads to the existence of two different Kondo temperatures.

In Fig. 6, we present spectral functions at smaller crystal-field splitting $\Delta_{cf}=\pm 0.1$ and at a fixed temperature. The effect of positive splitting $\Delta_{cf}=0.1$, when the doubly degenerate state lies below the fourfold-degenerate state, on the height of the central peak is stronger than in the opposite case at $\Delta_{cf}=-0.1$. The source of such behavior is the decrease of the Kondo temperature with a decrease of the effective degeneracy of the low-lying multiplet.[4,8] The side peak at $\omega>0$ increases as splitting changes from $\Delta_{cf}=0.0\rightarrow -0.1\rightarrow 0.1$. The later change is opposite to the change of the central $\omega\sim 0$ peak.

IV. CONCLUSION

Using the quantum Monte Carlo technique, we calculated the magnetic susceptibility and single-particle spectral density of the degenerate, single-impurity Anderson model in the case of spin-orbit and crystal-field splitting. To extract spectral properties by analytic continuation from the imaginary-time Green's function, we used the maximum entropy method combined with the principle of Bayesian statistical inference. In the case of spin-orbit splitting, we split sixfold degenerate states into doubly degenerate $j_1=\frac{1}{2}$ states and higher-lying fourfold-degenerate $j_i=\frac{3}{2}$ states. Such a splitting does not fully represent real spin-orbit splitting in the Ce impurity, where $N=14$ f states split into $N=6$ with $j=\frac{5}{2}$ and $N=8$ with $j=\frac{7}{2}$. However, with our present resources, we are limited to degeneracy $N=6$. In the case of crystal-field splitting, we were able to simulate a real physical situation where the low-lying $N=6, j=\frac{5}{2}$ states split into doubly degenerate Γ_7 and fourfold-degenerate Γ_8 states.

The magnetic susceptibility $T\chi_{so}$ calculated from states $j_1=\frac{1}{2}$ and $j_2=\frac{3}{2}$ displays a nonuniversal behavior in the intermediate temperature range at $\Delta_{so}=0$. The observed structure is simply a consequence of decreasing average f occupancy. As hybridization increases, the structure becomes less pronounced due to stronger screening of the local moment. Similar nonuniversal behavior is also found in the case of magnetic susceptibility $T\chi_{cf}$ calculated from the eigenstates of the cubic-crystal-field symmetry Γ_7 and Γ_8. In fact, when normalized to their high-temperature values, $T\chi_{so}$ and $T\chi_{cf}$ show similar behavior as a function of temperature $\Delta_{so}=\Delta_{cf}=0$. The situation changes dramatically at finite splittings $\Delta_{so}=\Delta_{cf}=0.3$: Spin-orbit splitting changes the behavior of $T\chi_{so}$ substantially, while the same magnitude of crystal-field splitting has almost no effect on $T\chi_{cf}$. We attribute such a small effect in the case of crystal-field splitting to a special redistribution of average occupancy of the states with different j_z within the eigenstates of Γ_7 and Γ_8.

The overall behavior of the spectral functions without any splitting follows predictions of NRG and NCA calculations. The central (Kondo) peak increases as temperature is lowered. With increasing interaction U, the central peak increases at a fixed temperature and the position of the $f^1\rightarrow f^2$ peak scales as $\omega\sim\epsilon_f+U$. We observed a slight temperature dependence of this peak. The side peak at negative frequencies $\omega\sim\epsilon_f$ is much less pronounced than its $f^1\rightarrow f^2$ counterpart. When splitting is switched on, the spectral weight of the central peak decreases as a consequence of lower Kondo temperature. The lost spectral weight at small frequencies is absorbed in the $f^1\rightarrow f^2$ peak. At large splitting $\Delta_{so}=0.3$, corresponding to spin-orbit splitting, we found a rather unusual temperature dependence of the central peak. In contrast to the usual expectations, the height of the central peak decreases with decreasing temperature in the temperature range above the Kondo temperature. We speculate that this behavior is due to the existence of two different low-energy scales in the system.

In the case of smaller crystal-field splitting, with $\Delta_{cf}=0.1$, we found that the effect of the crystal-field splitting on the low-energy spectrum is more pronounced when the low-lying multiplet has a smaller degeneracy. Thus we confirmed previous results of Sakai,[4] based on Schlottmann's predictions, that the Kondo temperature scales as the effective hybridization of the low-lying multiplet.

ACKNOWLEDGMENTS

This work was supported by the U.S. Department of Energy. We acknowledge helpful discussions with A. Arko.

[1]P. W. Anderson, Phys. Rev. **124**, 41 (1961).

[2]H. R. Krishna-murty, J. W. Wilkins, and K. G. Wilson, Phys. Rev. B **21**, 1003 (1980); **21**, 1044 (1980).

[3]A. M. Tsvelik and P. B. Wiegmann, Adv. Phys. **32**, 453 (1983).

[4]O. Sakai, Y. Shimizu, and T. Tasuya, J. Phys. Soc. Jpn. **58**, 3666 (1989).

[5]N. E. Bickers, D. L. Cox, and J. W. Wilkins, Phys. Rev. B **36**, 2036 (1987); N. E. Bickers, Rev. Mod. Phys. **59**, 845 (1987). For alternative approaches, see, for example, O. Gunnarsson Phys. Rev. B **28**, 4315 (1983); N. Read and D. M. Newns, J. Phys. C **16**, 3273 (1982).

[6]T. A. Costi and A. C. Hewson, Physica B **163**, 179 (1990); Physica C **185-189**, 2649 (1991); Philos. Mag. B **65**, 1165 (1992); J. Magn. Magn. Mater. **108**, 129 (1992).

[7]K. Yamada, K. Yoshida, and K. Hanzawa, Prog. Theor. Phys. **71**, 450 (1983).

[8]P. Schlottmann, Phys. Rev. B **30**, 1454 (1984).

[9]H. Q. Lin and J. E. Hirsch, Phys. Rev. B **37**, 1864 (1988).
[10]J. E. Hirsch and R. M. Fye, Phys. Rev. Lett. **56**, 2521 (1986).
[11]K. Takegahara, J. Phys. Soc. Jpn. **62**, 1736 (1992).
[12]K. R. Lea, M. J. M. Leask, and W. P. Wolf, J. Phys. Chem. Solids **23**, 1381 (1962).
[13]J. E. Gubernatis, R. N. Silver, and M. Jarrell, Phys. Rev. B **44**, 6011 (1991).
[14]J. Bonča and J. E. Gubernatis, Phys. Rev. B **47**, 13 137 (1993).
[15]R. K. Bryan, Euro. Biophys. J. **18**, 165 (1990).